Progress In Electromagnetics Research, PIER 86, 53–70, 2008

DESIGN AND CONSTRUCTION OF A NEAR REAL-TIME ADVANCED AUTOMATED C-BAND SCATTEROMETER SYSTEM

K.-S. Lim and V.-C. Koo

Faculty of Engineering
Multimedia University
63100 Cyberjaya, Malaysia

Abstract—This paper presents the design and construction of a complete near real-time scatterometer system for in-situ measurement. The full polarimetric system is comprised of inexpensive Frequency Modulated Continuous Wave (FMCW) radar that is efficiently constructed from a combination of commercially available components and in-house fabricated circuitry. An automated advanced antenna positioning system (AAPS) is included in the development of the system, giving rise for a more practical measurement. The backscattering matrices of a $4'' \times 8''$ dihedral corner reflector are rotated and measured at different angles to provide different sets of polarimetric data. The backscattering matrices of $8''$ sphere, $12''$ sphere and $16.5''$ trihedral are also measured and the results are presented in this paper. In order to verify the effectiveness of the calibration technique, the results are compared with the theoretical values. Consideration on the challenges of measurement in outdoor environment is countered with external and internal calibration. As a result, the proposed scatterometer system has shown good correlation between measurement and theoretical results.

1. INTRODUCTION

Remote sensing is well-known for its capability of providing complementary information to existing ground-based environmental monitoring systems. By means of microwave remote sensing technology, it offers timely information that allows us to measure, monitor, and analyse the time sequential changes of earth terrain. Hence, there is a strong need for effective means to develop

scatterometer in order to provide up-to-date, detailed information about land condition with its backscattering matrices.

Over the past few decades, there has been a considerable number of researchers who investigated the design and development of scatterometer for various monitoring applications [1–10]. Field scatterometers were employed at 10 GHz (X-band) [1, 11], while other studies [12–17] used 4.75 GHz field scatterometers and the microwave scatterometer C-band (MS-C). Investigation on the radar backscatter from the rice crops was done by Le-Toan [18, 19] by using an airborne X-band Synthetic Aperture Radar (SAR), VARAN-S, operating in HH and VV at the incident angles of 0° to 60°. Apart from that, Kurosu [20] had also conducted an experiment on the entire rice growth cycle with VV polarization at the incident angle of 23° while Kim [21] performed the measurements using X-band scatterometer. It appears from the literature that the radar backscattering coefficient varies with the measurement system used, and with the growth stage, due to the different physical structure of the rice plants. This variation may also be due to the difference in frequencies and incident angles. A ground-based C-band scatterometer was also constructed and installed on a mobile telescopic truck platform with the purpose of in-situ scattering measurements [22]. The FMCW radar, operating at a center frequency of 6 GHz faced various application and practical challenges during the outdoor in-situ measurement throughout the decade of continuous research. With this realization and as the scientific application of scatterometer data expands, the need for better scatterometer instrument designs is therefore crucial. Thus, in this paper, a complete refurbishment and remanufacturing have been proposed and performed on the existing scatterometer to accommodate for a more practical solution of measurement as well as improvement on the overall system stability and the data provision of dynamic range. The complete design of the proposed inexpensive scatterometer system with practically and stability consideration is presented for the first time.

The paper is outlined as follows. Section 2 describes the design and configuration of the ground-based FMCW microwave radar scatterometer with its detailed specification. This is followed by the explanation of the advanced antenna positioning system (AAPS) and FMCW integration in Section 3. In Section 4, the calibration processes are described with the detailed experimental procedures and measurement setup. The results are discussed in Section 5. In Section 6, we conclude and summarize this work.

2. DESIGN AND CONFIGURATION OF THE GROUND-BASED FMCW MICROWAVE RADAR SCATTEROMETER

A ground-based C-band scatterometer was constructed previously [22] with latching Radio Frequency (RF) switch that required additional driver circuit. This switch, however, has been replaced with TTL controllable RF switch in the proposed system in order to simplify the control design and ease the control mechanism. Furthermore, in order to reduce system interference, the flexible RF cables has been replaced with the better performance semi rigid cables. By replacing the cables and re-arranging the location of the RF discrete components, the sharp turns of the RF cables can be eliminated and consequently the internal reflection is reduced with good stability of the RF circuitry. The previous C-band scatterometer was mainly served as the experimental and proof of concept purposes and it did not consider practical commissioning challenges. Based on the difficulties experienced throughout the installation and commission using the previous system, careful consideration has been made on the mechanical mounting and RF terminal connection of the scatterometer. As a result, the newly refurbished system is able to reduce its setup time from half an hour to less than 10 minutes.

In order to give a better illustration of the changes made, the block diagrams of the previous and proposed systems are shown in Figure 1

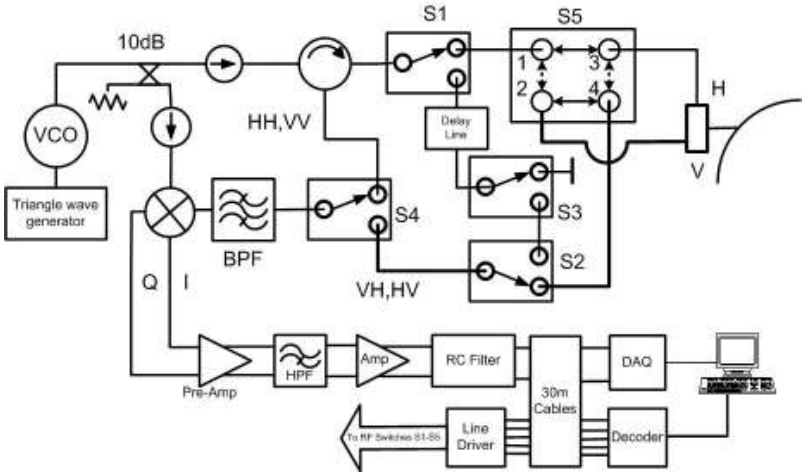

Figure 1. Block diagram of the previous C-band scatterometer system.

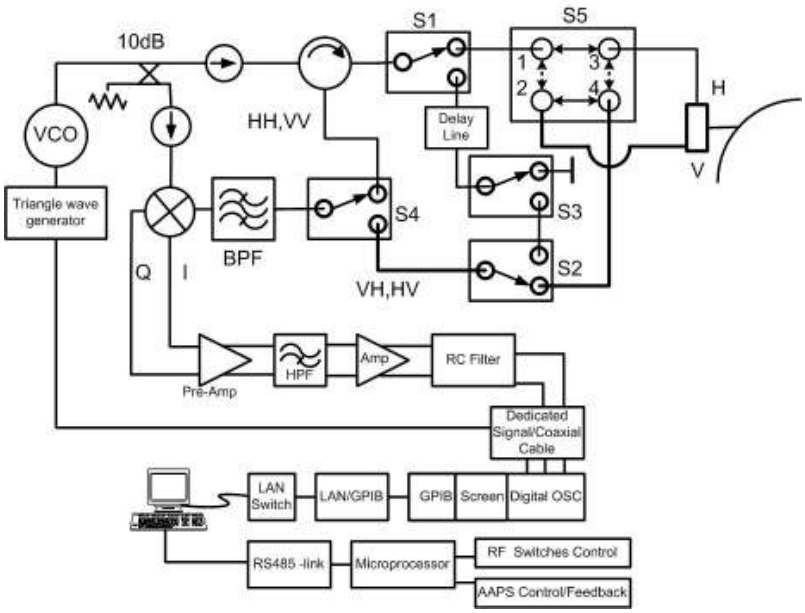

Figure 2. Block diagram of the proposed C-band scatterometer system.

and Figure 2, respectively. The comparison between the previous and proposed scatterometer systems are shown in Table 1. These differences range from the system mounting to the connections between RF block set and antenna. In the previous system which utilized in-house integrated microprocessor based Data Acquisition Unit (DAU) and control, challenges of the EMI noise coupled with the noise from digital and analog circuits were inevitable. The data recording was done through sample and hold circuit and data was then converted to radar backscattering coefficient. Thus, the process was time-consuming and it was not suitable for real-time processing. To surmount the problem, the proposed system introduces the data recording process using the industrial available, high speed digital oscilloscope that confers a host of benefits over a simple DAU card. It provides not only a wide range of dynamic data but also serves as the troubleshooting tools. Information such as frequency and voltage waveform can be obtained from the oscilloscope and radar return can be estimated first hand before it is processed. Unlike the conventional scatterometer system, the proposed system uses Ethernet based General Purpose Interface Bus (GPIB) connection linked oscilloscope as DAU which enables near

Table 1. System specifications of previous and proposed C-band scatterometer designs.

System Specifications	Previous System	Proposed System
System modulating technique	FMCW	FMCW
Operating frequency	6GHz	**6.235Ghz**
Operating wavelength	5cm	**4.8cm**
Sweep bandwidth	400MHz	**582MHz**
Modulating frequency	60Hz	**50Hz**
Polarization	HH,VV,HV,VH	HH,VV,HV,VH
Polarization isolation	35dB	35dB
Antenna gain	35dB	35dB
Antenna 3dB beamwidth	3 degree	3 degree
Best possible range resolution	0.375m	**0.257m**
Platform	mobile boom truck	mobile boom truck
Platform height	25meter	25meter
Measurement process	manual	**automated antenna positioner**
Data collecting time for 560 Samples	3 hours	**45 minutes**
Sample and hold (sample/second)	100K (Fix)	**250K typ. 5G Max**
Measurement Capability	**Previous System**	**Proposed System**
Transmit power	10dBm	10dBm
Received power	-15dBm to -92dBm	-15dBm to -92dBm
RCS dynamic range	+20dB to -40dB	+20dB to -43dB
Measurement range R	20 to 100 m	20 to 100 m
Incident angle coverage	0-70	0-70
Miminum SNR	10dB	10dB
Effective range resolution	Variable ~1.8m at 45 degree 4.5m at 50 degree	Variable ~1.8m at 45 degree 4.5m at 50 degree

real-time measurement. The fast response of the oscilloscope and data transfer from the oscilloscope buffer to the workstation uses less than 0.4 second where the preliminary result can be observed in time domain signal from the oscilloscope. With the commonly available oscilloscope, the system can be upgraded easily with newer released equipments. Apart from that, the usage of Ethernet based GPIB connection in the proposed system allows better accessibility and it is now possible to access the system remotely through wireless LAN.

3. ADVANCED ANTENNA POSITIONING SYSTEM AND FMCW INTEGRATION

The ground-based C-band scatterometer is installed on a mobile telescopic truck platform with the purpose of in-situ scattering

Figure 3. Antenna mounting in previous scatterometer system.

measurements. In most of the measurement campaigns, an average of 20 samples is recommended for every incident angle to obtain reliable results. As the antenna was statically attached to the telescopic boom in the previous system as shown in Figure 3, the telescopic boom had to be adjusted manually by human operator to different location and angle for independent data collection. Besides, there was frequent vibration occurred, causing unwanted noise in the radar backscattering measurement. Hence, an advanced antenna positioning system (AAPS) is integrated to overcome the problems mentioned. The AAPS is depicted in Figure 4.

Figure 4. AAPS installed on the proposed scatterometer system.

Several criteria have been considered for the integration. These include the maximum load of the telescopic boom, limitation of the horizontal length of the mobile platform to store the automation and integration between AAPS and its electronics control system for the motor movement control. To accommodate the maximum load of the telescopic boom, the AAPS has been designed and fabricated within 100 Kg which is 50% of the maximum load allowed by the telescopic manufacturer. The maximum horizontal length is fixed at 2 meter as the maximum horizontal width of the mobile platform is at 2.3 meter. On the other hand, the resolution of the horizontal scan is fixed at 1 cm and the angular resolution is set at 0.5 degree. To reduce the potential EMI interference and noise, an EMI filter has been employed as the main EMI power filter since the power is generated by a diesel engine-generator set. An additional EMI filter is also installed on a separate power supply that provides power to VCO, RF and signal conditioning circuitry to further filter the noise generated from the motorized AAPS.

In order to perform a fully automated radar backscattering measurement, an additional microcontroller is designed and installed on the control panel of the AAPS. The microcontroller is programmed as secondary processor to execute operation requests from the main workstation. These requests include scatterometer operation sequences, movement of the AAPS in horizontal direction, update of the status of the system and movement of the antenna pointing angle. The main workstation and the microcontroller are linked up with a RS485 standard communication channel to ensure its stability during measurement.

As shown in Figure 2, a quadrature mixer is used to provide two intermediate frequency signals namely In-phase (I) signal and a Quadrature-phase (Q) signal to provide both magnitude and phase information from the measured target. Therefore, two dedicated coaxial cables is utilized to transfer both frequency signals to the control cabin for data recording while an additional data cable link is installed to deliver a feedback signal from the VCO modulating circuitry for system monitoring purpose.

With this tremendous improvement, the proposed C-band scatterometer have sped up the measurement time from 3 hours to 45 minutes for a typical 560 data collection. This is crucial for outdoor measurement campaign in fast changing weather countries.

4. SYSTEM CALIBRATION

The absolute calibration of the backscattering signal of a scatterometer is important for the retrieval of optimum quality geophysical data. The procedures employed in performing the calibration and measurements are similar with the previous work [22]. The internal calibration is performed by comparing the measured target response with a 100 ns delay line response. In the external calibration process, the relative measurement is matched to the theoretical value to obtain an error correction factor. The system is, then, verified using two standard radar point targets namely trihedral and dihedral corner reflectors. The correction factor is used to convert the relative measurement of the point target to its absolute value and the calibrated data is compared with the theoretical value for verification.

In this paper, four standard test targets are involved in the experiment setup. These include 8″ conducting sphere, 12″ conducting sphere, 4″ × 8″ dihedral and 16.5″ trihedral corner reflectors. Both external and internal calibrations are conducted to eliminate the system noise in the measurements. For the internal calibration, a 100 ns delay line is incorporated in the scatterometer. Hence, the scatterometer is able to obtain a return target at 15 meter and 30 meter for cross-polarization and co-polarization modes based on the designated system. External calibration is accomplished with the measurement of a metal sphere to perform full polarimetric calibration for all linear polarizations [23].

Full polarimetric measurements on metal sphere, dihedral and trihedral corner reflectors are measured to verify the measurement accuracy. To reduce scattering due to the pedestal, a 2.6 meter height tower made out of Styrofoam column with dielectric close to unity are build as the pedestal to support the radar point target. During the experiment, the distance between the antenna and the pedestral is set to be 23 meter as depicted in the Figure 5.

Figure 5. Experimental setup for calibration purpose.

5. RESULTS AND DISCUSSION

The radar cross section (RCS) of the radar point target is measured and compared with the theoretical value to verify on the effectiveness of the measurement. TThe measured results of of the $8''$ sphere, $12''$ sphere, $\alpha = 0°$ oriented $4'' \times 8''$ dihedral, $\alpha = 90°$ oriented $4'' \times 8''$ dihedral and $\alpha = 45°$ oriented $4'' \times 8''$ dihedral point targets are shown in Figure 6, Figure 7, Figure 8, Figure 9, Figure 10 and Figure 11, respectively. These results include power spectral density, phase and magnitude responses and backscattering coefficient of each point targets.

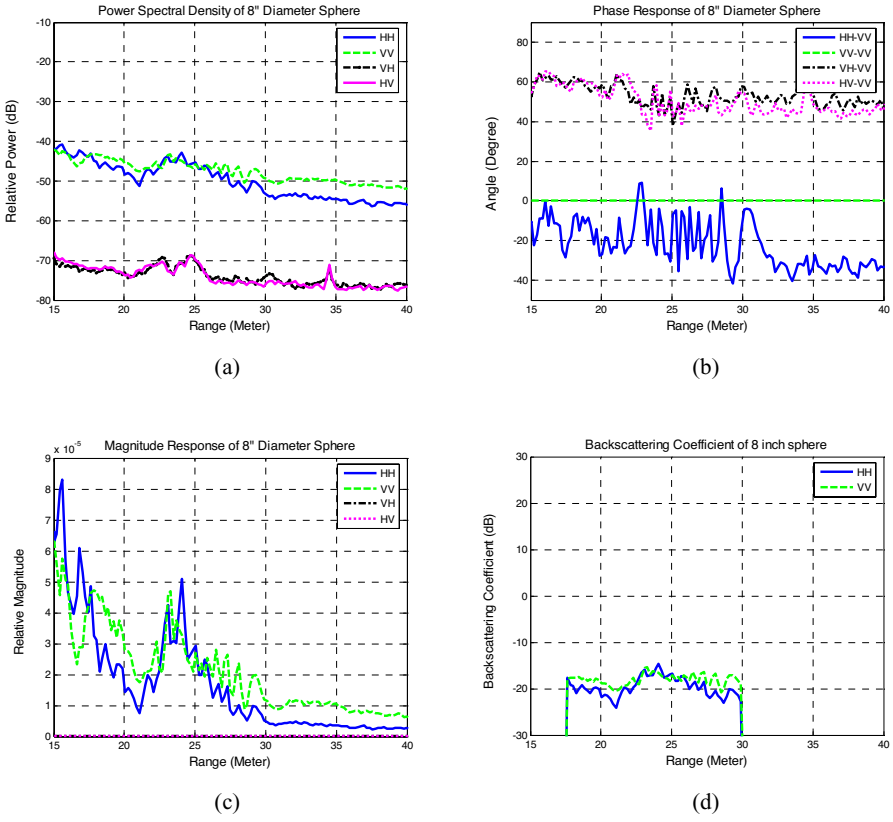

Figure 6. Target responses of $8''$ sphere.

As shown in Figure 6(a) and Figure 7(a), at the target range of 23 meter, the power spectral density of the $8''$ and $12''$ are relatively smaller than the rest of the radar point targets in Figure 8(a) and Figure 9(a). This is agreeable with the theoretical value where $8''$ and

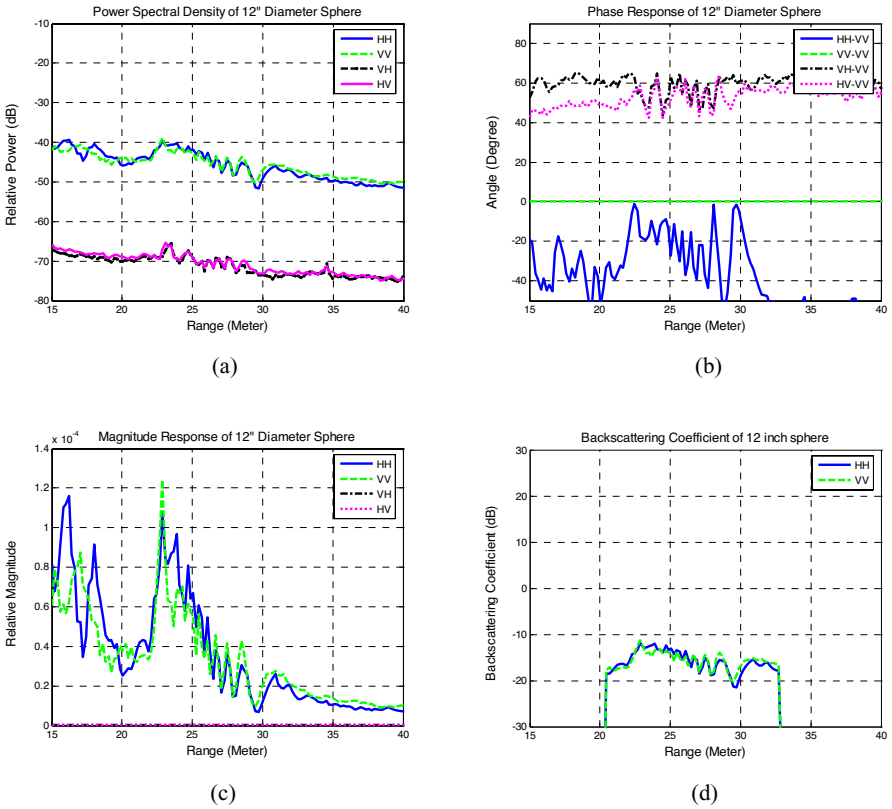

Figure 7. Target responses of 12″ sphere.

12″ spheres have smaller RCS values than a 4″ × 8″ dihedral corner reflector by 20 dB and 17 dB, respectively. However, with the aid of magnitude response from Figure 6(c) and Figure 7(c), the target returns of 8″ and 12″ sphere at 23 meter are able to identified clearly. Two strong target returns can be observed at the range of 16 meter and 17.5 meter and these are mainly due to internal reflection. The power spectral density response is then recalculated to radar backscattering coefficient. The truncations shown in Figure 6(d), Figure 7(d), Figure 8(d), Figure 9(d), Figure 10(d) and Figure 11(d) are due to predefined gating in order to eliminate the unwanted reflection. The radar backscattering coefficient shown in Figure 6(d) and Figure 7(d) display close agreement with the theoretical value. Phase response of the 8″ and 12″ spheres are depicted in Figure 6(b) and Figure 7(b). The phase response of these spheres shows some variations and fluctuations and

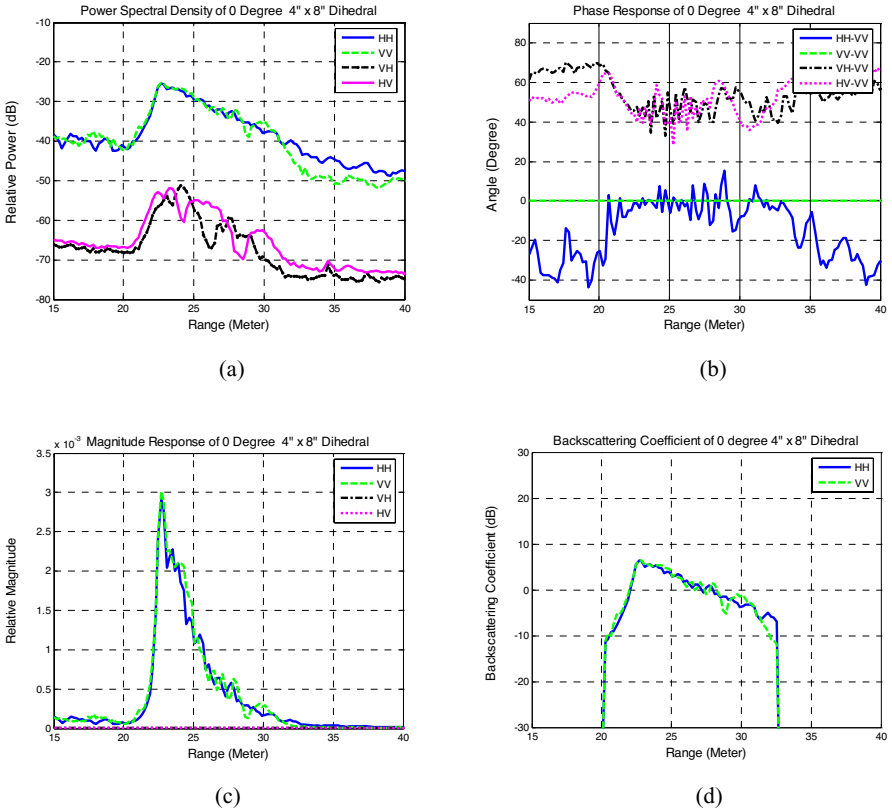

Figure 8. Target responses of $4'' \times 8''$ dihedral with $\alpha = 0°$ orientation.

these are probably caused by the phase noise contamination.

Figure 8, Figure 9 and Figure 10 show the radar return from $4'' \times 8''$ dihedral with $\alpha = 0°$, $\alpha = 90°$ and $\alpha = 45°$ orientation, respectively. The power spectral density responses from Figure 8(a) and Figure 9(a) and magnitude responses in Figure 8(c) and Figure 9(c) show strong radar return from co-polarization (HH and VV mode). This is agreeable with the theoretical model of dihedral that the target returns occur in co-polarization at orientation of $\alpha = 0°$ and $\alpha = 90°$. The phase responses in Figure 8(b) and Figure 9(b) show better stability that are close to 0° at the target range. This may be due to a stronger return from the dihedral corner reflector compared to metal spheres. However, a weak leakage signal is detected in the cross-polarized mode (VH and HV). This phenomenal is most probably due to the antenna cross talk contamination. It is found that the

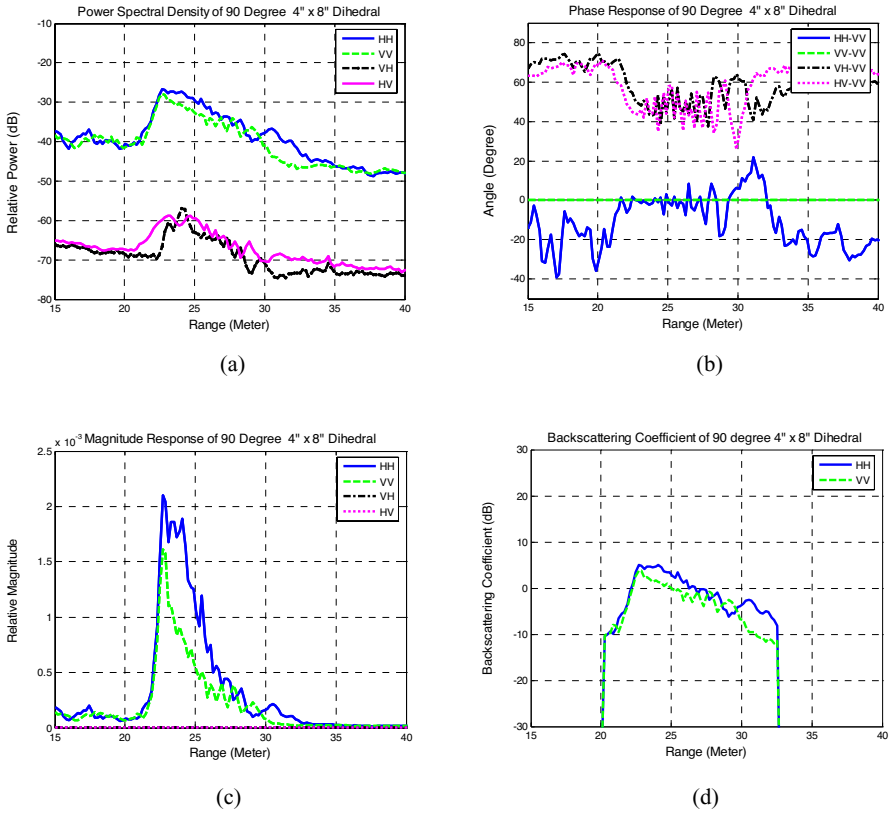

Figure 9. Target responses of $4'' \times 8''$ dihedral with $\alpha = 90°$ orientation.

backscattering values show a close agreement to the theoretical value of 6.3 dB.

Figure 10(a) and Figure 10(c) observe strong cross polarization (VH and HV) returns from $\alpha = 45°$ oriented $4'' \times 8''$ dihedral in power spectral density and magnitude responses. It is found that these values are similar to the theoretical target responses of the dihedral oriented at $\alpha = 45^o$. The phase response in Figure 10(b) and radar backscattering in Figure 10(d) display good agreement with the theoretical value. On the other hand, Figure 11 shows responses of a $16.5''$ trihedral corner reflector. There is a strong return at 23 meter in HH and VV mode as depicted in Figures 11(a) and 11(c). The phase responses in Figure 11(b) are almost 0° at target range with some fluctuations at this distance. The radar backscattering of the $16.5''$ trihedral corner

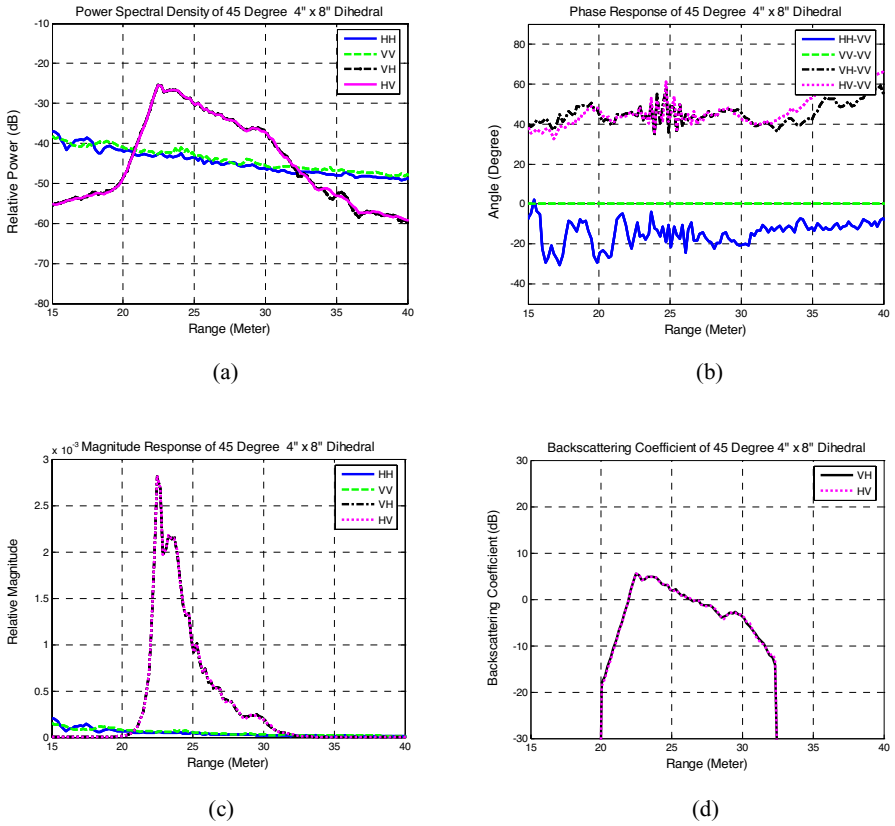

Figure 10. Target responses of $4'' \times 8''$ dihedral with $\alpha = 45°$ orientation.

reflector shown in Figure 11(d) is also agreeable with the theoretical value of 17.8 dB.

The measurement accuracy is evaluated by comparing the measured results with the theoretical values. The errors associated with the RCS magnitude in dB and phase measurement are summarized in Table 2 and Table 3, respectively. Some of the theoretical values of RCS point targets are minus infinity ($-\infty$ dB) of which they are impossible to be achieved in practical instrument. Therefore, a leakage signal of less than 26 dB from the actual measured result can be observed in the measurements shown in this paper. These are probably caused by the antenna cross-polarization isolation and background clutter. In general, it is observed that the measurement accuracy is within ± 1.5 dB in magnitude and $\pm 10°$ in phase.

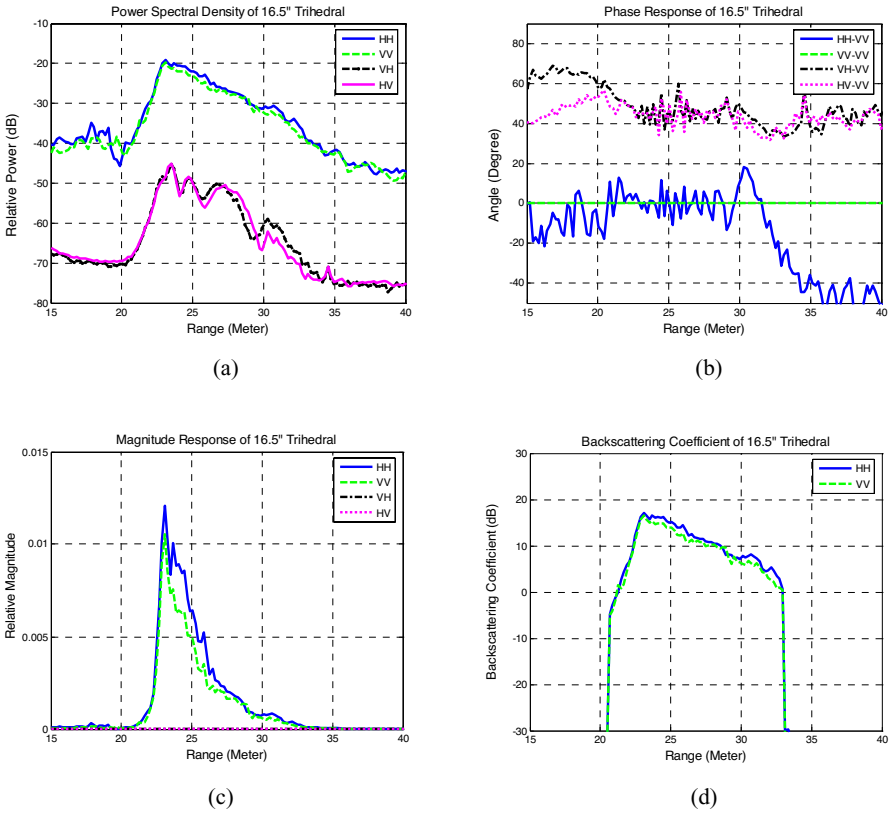

Figure 11. Target responses of 16.5″ trihedral.

Table 2. Magnitude error associated with RCS measurements.

	VV	HH	HV	VH
Trihedral	–1.35	–0.76	--	--
Dihedral 0 °	–1	–1.15	--	--
Dihedral 45 °	--	--	–0.76	–0.84
Dihedral 90 °	1.5	–0.4	--	--
Sphere 12"	–1.2	–0.3	--	--
Sphere 8"	–0.3	0.2	--	--

Table 3. Phase error associated with RCS measurements.

	HH-VV (^{O})	HV-VV (^{O})	VH-VV (^{O})
Trihedral	–2.3	--	--
Dihedral 0 ^{O}	–1.2	--	--
Dihedral 45 ^{O}	--	– 0.9	1.8
Dihedral 90 ^{O}	0.1	--	--
Sphere 12''	–10	--	--
Sphere 8''	– 8	--	--

6. CONCLUSIONS

A near real-time scatterometer has been successfully designed and installed onto a telescopic boom truck with an automated antenna positioning system. The system operates at C-band (6.235 GHz) with wide bandwidth (582MHz) and large incident angle coverage ranging from 0° to 70°. Both internal and external calibrations have been conducted and it is observed that the measurement accuracy is within ±1.5 dB in magnitude and ±10° in phase. Rice field measurement campaign was conducted from 2007–2008 at Sungai Burung, Selangor, Malaysia. Some promising results on rice growth have been reported in [24–26]. As compared to the previous system, this new scatterometer has better range resolution, faster data collection time, and a fully automated antenna positioning control system. In near future, the scatterometer will be employed to conduct a series of in situ measurements on rice fields and oil palm plantations in Malaysia.

ACKNOWLEDGMENT

This research work is a collaboration work between Multimedia University, Malaysia and Malaysian Remote Sensing Agency (MACRES). The cooperation of the authorities from Ministry of Agriculture during the field measurements and calibration is also appreciated.

REFERENCES

1. Rakotoarivony, L., O. Taconet, D. Vidal-Madjar, P. Bellemain, and M. Benallegue, "Radar backscattering over agricultural

bare soils," *Journal of Electromagnetic Waves and Applications*, Vol. 10, No. 2, 187–209, 1996.

2. De Carolis, G., F. Mattia, G. Pasquariello, F. Posa, and P. Smacchia, "X-band SAR and scatterometer data inversion based on geometrical optics model and Kalman filter approach," *Journal of Electromagnetic Waves and Applications*, Vol. 8, No. 8, 1017–1039, 1994.
3. Storvold, R., E. Malnes, Y. Larsen, K. A. Høgda, S. E. Hamran, K. Müller, and K. A. Langley, "SAR remote sensing of snow parameters in norwegian areas — Current status and future perspective," *Journal of Electromagnetic Waves and Applications*, Vol. 20, No. 13, 1751–1759, 2006.
4. Albert, M. D., T. E. Tan, H. T. Ewe, and H. T. Chuah, "A theoretical and measurement study of sea ice and ice shelf in antarctica as electrically dense media," *Journal of Electromagnetic Waves and Applications*, Vol. 19, No. 14, 1973–1981, 2005.
5. De Badereau, D., H. Roussel, and W. Tabbara, "Radar remote sensing of forest at low frequencies: A two dimensional full wave approach," *Journal of Electromagnetic Waves and Applications*, Vol. 17, No. 6, 921–949, 2003.
6. Li, Z. X., "Modelling the passive microwave remote sensing of wet snow," *Progress In Electromagnetics Research*, PIER 62, 143–164, 2006.
7. Boyarskii, D. A., V. V. Tikhonov, and N. Y. Komarova, "Model of dielectric constant of bound water in soil for applications of microwave remote sensing," *Progress In Electromagnetics Research*, PIER 35, 251–269, 2002.
8. Angot, L., H. Roussel, and W. Tabbara, "A full wave three dimensional analysis of forest remote sensing using VHF electromagnetic wave," *Progress In Electromagnetics Research*, PIER 38, 311–331, 2002.
9. Nghiem, S. V., M. Borgeaud, J. A. Kong, and R. T. Shin, "Polarimetric remote sensing of geophysical media with layer random medium model," *Progress In Electromagnetics Research*, PIER 03, 1–73, 1990.
10. Shin, R. T. and J. A. Kong, "Radiative transfer theory for active remote sensing of two-layer random medium," *Progress In Electromagnetics Research*, PIER 01, 359–417, 1989.
11. Picard, G. and T. Le Toan, "A multiple scattering model for C band backscatter of wheat canopies," *Journal of Electromagnetic Waves and Applications*, Vol. 16, No. 10, 1447–1466, 2002.

12. Paris, J. F., "Active microwave properties of vegetation," *Fund. Remote Sensing Sci. Res. Program, 1985 Summary Report of the Scene Radiation and Atmos. Effects Characterization Project*, D. Deering (ed.), 148–154, NASA TM 86234, M.I.T., Cambridge, MA, 1985.
13. Paris, J. F., "Characterization of cultural deciduous trees, grapes, and irrigated crops with radar and optical remote sensing," *Ann. Rep., Microwave-optical Characterization of Vegetation with Remote Sensing Project*, NASA Lyndon B. Johnson Space Center, Houston, TX, 1985.
14. Paris, J. F., "Radar scatterometer probing of thick vegetation canopies," *International Geoscience Remote Sensing Symposium*, Vol. 1, 161–163, 1985.
15. Pitts, D. E., G. D. Badhwar, and E. Reyna, "Estimation of biophysical properties of forest canopies through inversion of microwave scatterometer data," *International Geoscience Remote Sensing Symposium*, Vol. 1, 313–320, 1985.
16. Wu, S. T., "A preliminary report on the measurements of forest canopies with C-band radar scatterometer at NASA/NSTL," *International Geoscience Remote Sensing Symposium*, Vol. 2, 168–173, 1985.
17. Lopez-Sanchez, J. M., J. Fortuny-Guasch, S. R. Cloude, and A. J. Sieber, "Indoor polarimetric radar measurements on vegetation samples at L, S, C and X band," *Journal of Electromagnetic Waves and Applications*, Vol. 14, No. 2, 205–231, 2000.
18. Le Toan, T., H. Laur, E. Mougin, and A. Lopes, "Multitemporal and dual-polarization observations of agricultural vegetation covers by X-band SAR images," *IEEE Transactions on Geoscience and Remote Sensing*, Vol. 27, 709–717, 1989.
19. Le Toan, T., F. Ribbes, L. F. Wang, N. Floury, K. H. Ding, J. A. Kong, M. Fujita, and T. Kurosu, "Rice crop mapping and monitoring using ERS-1 data based on experiment and modeling results," *IEEE Transactions on Geoscience and Remote Sensing*, Vol. 35, 41–56, 1997.
20. Kurosu, T., M. Fujita, and K. Chiba, "Monitoring of rice crop growth from space using ERS1 C-band SAR," *IEEE Transactions on Geoscience and Remote Sensing*, Vol. 33, 1092–1096, 1995.
21. Kim, S. B., B. W. Kim, Y. K. Kong, and Y. S. Kim, "Radar backscattering measurements of rice crop using X-band scatterometer," *IEEE Transactions on Geoscience and Remote Sensing*, Vol. 38, 1467–1471, 2000.

22. Koo, V. C., B. K. Chung, and H. T. Chuah, "Development of a ground-based radar for scattering measurements," *IEEE Antennas and Propagation Magazine*, Vol. 45, No. 2, 36–42, 2003.
23. Sarabandi, K. and F. T. Ulaby, "A convenient technique for polarimetric calibration of single-antenna radar systems," *IEEE Transactions on Geoscience and Remote Sensing*, Vol. 28, 1022–1033, 1990.
24. Lim, K. S., C. P. Tan, J. Y. Koay, V. C. Koo, H. T. Ewe, Y. C. Lo, and A. Ali, "Multitemporal C-band radar measurement on rice fields," *Progress in Electromagnetic Research Symposium*, Beijing, March 2007.
25. Koay, J. Y., K. S. Lim, H. T. Ewe, H. Jamil, S. Bahari, and H. T. Chuah, "Preliminary study in the backscattering measurements and theoretical modeling of oil palm canopies," *The 28th Asian Conference on Remote Sensing*, Putra World Trade Center (PWTC), Kuala Lumpur, Malaysia, November 12–16, 2007.
26. Lim, K. S., V. C. Koo, H. Jamil, S. Saleh, A. Ali, S. Yusof, K. K. Ng, Z. Abdullah, S. M. Md Zin, and M. F. Abdul Rahman, "Correlation study between ground-based C-band mobile scatterometer system and RADARSAT on paddy field backscattering coefficient over sungai burung area," *The 28th Asian Conference on Remote Sensing*, Putra World Trade Center (PWTC), Kuala Lumpur, Malaysia, November 12–16, 2007.